4th International Conference on Structural Integrity and Durability, ICSID 2020

Application of Design of Experiments to Foreign Object Damage on 7075-T6

Emanuele Vincenzo Arcieri[a], Sergio Baragetti[a]*, Željko Božić[b]

[a]Department of Management, Information and Production Engineering, University of Bergamo, Viale Marconi 5, Dalmine 24044, Italy
[b]Faculty of Mechanical Engineering and Naval Architecture, University of Zagreb, I. Lučića 5, Zagreb 10000, Croatia

Abstract

In this work, Design of Experiments is applied to identify which factors mostly influence the residual stress distribution in an hourglass specimen subject to the impact of a foreign object. The specimen is made of 7075-T6, that is one of the most popular alloys in the aeronautical sector. After the impact, the specimen is assumed to be tested with an axial or bending fatigue load. For this reason, the study is conducted on the axial stresses induced by the impact of the object on the specimen, assessed by means of finite element analysis. Only the stresses in the region x=[-2 mm; 2 mm], with x=0 corresponding to the position of the minimum cross section of the specimen before the impact, were considered. In this region, stress concentrations are probable during the fatigue test. The results showed that high impact forces induce high tensile stresses, unfavorable from a fatigue point of view. Therefore, it is preferable that the impacting object has a low weight and reduced speed.

1. Introduction

   Lightweight alloys are attractive to the aeronautical sector, because they allow the fabrication of components with high specific strength. The higher the specific strength, the higher the performance, as the reduced mass of the components means low inertia and consequently low fuel consumption. For this reason, the Authors' research activity

* Corresponding author. Tel.: +39-035-205-2382; fax: +39-035-205-2221.
  E-mail address: sergio.baragetti@unibg.it

is focused on the characterization of these materials. The studies on titanium alloys are presented in Baragetti (2013), Baragetti et al. (2019a), and Baragetti et al. (2019b), the behavior of aluminum alloys is described in Baragetti et al. (2019c).

The components of the aeronautical industry must have a high stiffness and a high static and fatigue strength. Strength must be guaranteed in the presence of defects, which are always existent. It is essential to consider flaws in the design phase and monitor them in terms of shape and propagation speed. Defects are indeed possible nucleation sites for fatigue cracks that propagate and cause failures according to the mechanism reported in Božić et al. (2014), Mlikota et al. (2017), Babić et al. (2018), Mlikota et al. (2018), Božić et al. (2018) and Babić et al. (2019). This mechanism can be summarized as follows: (i) slip bands are formed as a consequence of the sliding on continuous crystallographic planes; (ii) pores nucleate and form micro cracks; (iii) micro cracks join to form macro cracks and (iv) cracks propagate until the failure. Fatigue can drastically reduce the life of a component as reported for instance in Papadopoulou et al. (2019). It is therefore mandatory to evaluate the fatigue life of the components and to propose methodologies to assess it. For this purpose, simulation is gradually assuming an important role because it allows to save time and setup cost. Some examples are reported in Pastorcic et al. (2019), Babić et al. (2020), Cazin et al. (2020), Solob et al. (2020) and Rølvåg et al. (2020).

As known, residual stresses affect the fatigue strength of the components. Residual stresses can be induced by the deposition of a coating as described in Baragetti et al. (2005) and Baragetti et al. (2020), by the implantation of chemical species as reported in Voorwald et al. (2019) and by the impact of objects. In this regard, it is mandatory to mention shot peening and Foreign Object Damage (FOD). Shot peening refers to a global effect, provided by the impact of a large number of objects. According to Nicholas (2006), FOD is a typical expression in the aerospace and aviation industry, indicating the damage of engine components due to the impact of alien objects ingested. The effect of the FOD is local. This paper investigates the residual stress distribution induced by the FOD on an hourglass specimen made of 7075-T6 aluminum alloy, which is one of the most widespread alloys in the aeronautical industry. The stresses are assessed by Finite Element (FE) modelling and Design of Experiments (DoE) is applied to the results to identify the best levels of the most important input data to minimize the (tensile) residual stress quickly and   cost-effectively.

| **Nomenclature**	
D	diameter of the ball
E	Young's modulus
E1	empty parameter 1
E2	empty parameter 2
i	run number
MSD	mean square deviation, measure of data dispersion
n	number of tests per run
R_s	yield stress
S11	stress in axial direction
S/N	signal to noise ratio, measure of both the location and dispersion of the measured effect
S/N'	average of S/N in which factor x is at level y
V	impact speed
X	position of the maximum axial stress in x direction, in the region x=[-2 mm, 2 mm]
Y'	average of σ in which factor x is at level y
α	impact angle measured on xz plane
β	impact angle measured on yz plane
ΔS/N'	modulus of the difference between S/N' at level 1 and S/N' at level 2 for the considered parameter
μ	coefficient of friction
ν	Poisson's ratio
ρ	density
σ	maximum axial stress in the specimen, in the region x=[-2 mm,2 mm]
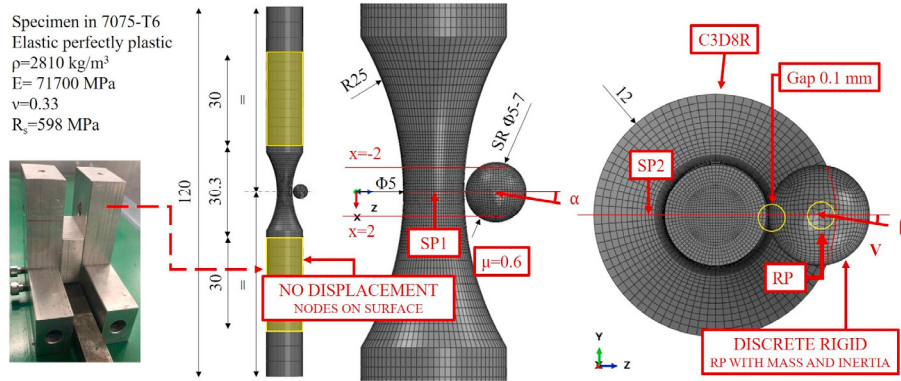
Fig. 1. FE model, adapted from Arcieri et al. (2021).

2. Materials and methods

DoE was applied to assess the most important factors and choose the preferred levels to minimize the residual stresses in the sample, which were evaluated with the FE models of Fig. 1. These models are similar to those of Arcieri et al. (2021) and they are described in the following lines. The Taguchi $L_8(2^7)$ array filled with the factors shown in Table 1 was employed. This array allows to optimize seven factors with only eight runs. The empty columns E1 and E2 allow to understand whether some parameter was not taken into account. A full description of the DoE methodology adopted is reported in Condra (1993), Baragetti (1997) and Baragetti and Terranova (2000).

Table 1. Taguchi $L_8(2^7)$ array: factors and respective levels.

Run	V (m/s)	Material of the ball	D (mm)	α (°)	β (°)	E1	E2
1	80	steel	5	0	0	1	1
2	80	steel	5	20	20	2	2
3	80	ceramic	7	0	0	2	2
4	80	ceramic	7	20	20	1	1
5	120	steel	7	0	20	1	2
6	120	steel	7	20	0	2	1
7	120	ceramic	5	0	20	2	1
8	120	ceramic	5	20	0	1	2

The impacts were studied by FE analysis in Abaqus Explicit 2019. Indeed, impact problems are usually solved using explicit integration schemes, as reported in Arcieri et al. (2018), Baragetti and Arcieri (2019), Baragetti and Arcieri (2020a) and Baragetti and Arcieri (2020b). In the models, the 7075-T6 specimen and the steel ball were positioned as shown in Fig. 1. The sample was modelled with 92160 linear hexahedral elements, C3D8R according to the Abaqus terminology. The global mesh size in the impact area was 0.25 mm. It was assumed that the behaviour of the material was elastic perfectly plastic, with the properties reported in the upper left corner of the figure. The ball was considered stiff, whatever the material. It was modelled with linear quadrilateral rigid elements, R3D4, with a global mesh size of 0.25 mm. The mass and moments of inertia were then assigned to the Reference Point (RP) of the ball, which was positioned at its centre. For the calculation of the inertial properties, it was assumed ρ=7860 kg/m³ for steel and ρ=2300 kg/m³ for ceramic. The ball was assumed to be fired close to the external surface of the specimen, with the RP lying in the same plane as the specimen's minimum cross-section, x=0, whatever the direction of impact. The minimum gap between the external surface of the sample and the external surface of the ball was 0.1 mm. The models did not consider the contribution of air to the movement of the ball. Due to the size of the ball and the specimen, the contribution of weight to the dynamics of the studied system and to the stress distribution was considered negligible. Therefore, gravity load was not implemented. The specimen was assumed to be located in the support shown in the lower left corner of Fig. 1, with its two cylindrical parts housed in the through holes and locked with two set screws. For this reason, the nodes on the external surface of the sample corresponding to the holes (yellow areas in Fig. 1) were locked. The symmetry conditions were implemented on the sample and on the RP of the ball

with respect to the planes of symmetry SP1 and SP2 of Fig. 1 whenever they were consistent with the impact direction analysed. A coefficient of friction μ=0.6 was set between the ball and the sample in all the eight runs. A dynamic step of 7 ms was adopted. At this time, the stresses in the sample can be considered stabilized.

3. Results and discussion

The specimen was assumed to be tested with an axial or bending fatigue load after impact. Both loading conditions provide an axial stress distribution and for this reason the residual stresses induced by the impact in the axial direction are considered in this paper. Tensile stresses are unfavorable from a fatigue point of view and for this reason the Taguchi method was used to identify the preferable levels of the most important parameters to minimize the tensile residual stresses. To do this, the maximum axial stress σ in the region x=[-2 mm, 2 mm], shown in Fig.1, was assessed for each run. Not the whole specimen, but only this region was considered because it is reasonable to assume that the maximum stresses will be reached here in the fatigue test. In this region, indeed, the cross-sectional areas are the smallest in the specimen and the notch induced by the impact provides stress concentrations.

Table 2 is called 'Response table' and it was built with the results shown in Fig.2. The table reports the results regarding the effect 'maximum axial stress' σ according to the Taguchi method. The maximum axial residual stresses for each run in x=[-2 mm, 2 mm] region are reported in the second column of the table. For each stress, it is indicated its position in x direction, X. As expected, X=0 mm for run 1, 3 and 7, where the x-component of the impact speed was zero. For Run 5, the maximum stress, 465 MPa, was at X=±3.5 mm, outside the considered region; considering the region x=[-2 mm, 2 mm], the maximum stress, 448 MPa, was at X=0 mm according to the symmetry of the problem. As the goal was to minimize the stresses, the results were analyzed according to the modality 'smaller is better' and MSD was calculated as MSD=$\sum\sigma_i^2/n$, assuming n=1 since one (deterministic) simulation per run was carried out. The calculation of S/N=-10log(MSD) and of Y' and S/N' for each level of each parameter allowed to identify V, Material and D as the most important factors, since ΔS/N' for these parameters is much greater than ΔS/N' for the others. For this reason, V, Material and D are in bold in Table 2. The preferred levels of the important parameters correspond to the highest values on S/N' and are underlined in Table 2: V=80 m/s, Material=ceramic and D=5 mm. The impact direction does not seem to be one of the most important factors for the residual stresses in x=[-2 mm, 2 mm]. Probably α and β are more effective once the post-impact stress concentrations associated to the notch created and the total stresses in the specimen subject to fatigue are assessed. The analysis of the empty columns confirmed that all the factors were taken into consideration. The F-test performed for the analysis of variance revealed that V, Material and D are significant with a confidence greater than 95%.

Table 2. Response table.

| Run	σ (*MPa*)	X (*mm*)	MSD (*MPa²*)	S/N	Parameters	Levels	Y' (*MPa*)	S/N'	ΔS/N'
1	198	0.0	3.920E+04	-45.933	**V**	<u>80 m/s</u>	224.000	-46.969	2.723
2	254	1.1	6.452E+04	-48.097		120 m/s	319.750	-49.692	
3	215	0.0	4.623E+04	-46.649	**Material**	steel	319.500	-49.651	2.642
4	229	1.0	5.244E+04	-47.197		<u>ceramic</u>	224.250	-47.010	
5	448	0.0	2.007E+05	-53.026	**D**	<u>5 mm</u>	226.250	-47.056	2.549
6	378	2.0	1.429E+05	-51.550		7 mm	317.500	-49.605	
7	219	0.0	4.796E+04	-46.809	α	0°	270.000	-48.104	0.453
8	234	0.8	5.476E+04	-47.384		20°	273.750	-48.557	
			--------------		β	0°	256.250	-47.879	0.903
			6.487E+05			20°	287.500	-48.782	
					E1	1	277.250	-48.385	0.109
						2	266.500	-48.276	
					E2	1	256.000	-47.872	0.917
						2	287.750	-48.789	
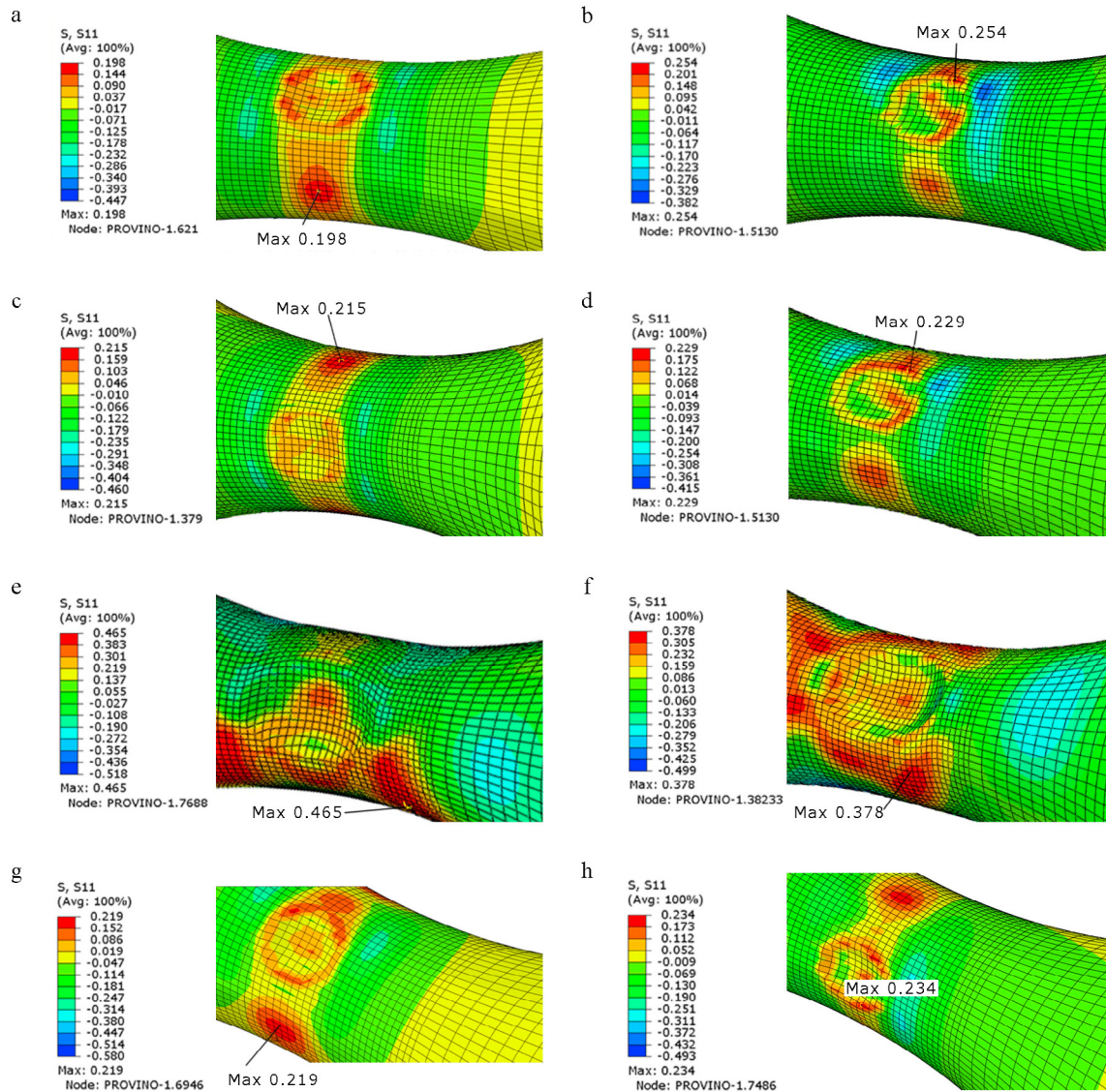
Fig. 2. Residual stresses (GPa) in axial direction: (a) Run 1; (b) Run 2; (c) Run 3; (d) Run 4; (e) Run 5; (f) Run 6; (g) Run 7; (h) Run 8.

The results therefore show that small impact forces are preferable to reduce the axial residual stresses in the sample in the region x=[-2 mm; 2 mm]. Material and D affect the mass of the ball and the product of the mass and V is its initial momentum. The greater the momentum, the greater the impact force and the greater the stresses, which are associated to a greater deformation.

A final consideration should be made on the values of stresses reached in the runs: Run 5 gives very high residual stresses that can be responsible for an early failure of the sample when the fatigue stresses are superposed. The high stresses reached can be due to the size of the ball, comparable to that of the sample, and the high impact speed.

4. Conclusions

In this work, DoE was applied to FE analyses to identify which factors mostly affect the residual stress distribution in a 7075-T6 hourglass specimen subject to the impact of a ball. Assuming an axial or bending fatigue stress

distribution after impact, only residual stresses in axial direction were considered. Only the stresses in the region x=[-2 mm; 2 mm] were considered because stress concentrations are expected here during the fatigue test. The results showed that small impact forces are preferable, that can be reached with a low impact speed and low ball mass.

References

Arcieri, E.V., Baragetti, S., Fustinoni, M., Lanzini, S., Papalia, R., 2018. Study and modelling of the passenger safety devices of an electric vehicle by finite elements. Procedia Structural Integrity 8, 212-219.

Arcieri, E.V., Baragetti, S., Lavella, M., 2021. Effects of FOD on fatigue strength of 7075-T6 hourglass specimens. IOP Conference Series: Materials Science and Engineering (submitted).

Babić, M., Verić, O., Božić, Ž., Sušić, A., 2018. Reverse engineering based integrity assessment of a total hip prosthesis. Procedia Structural Integrity 13, 438-443.

Babić, M., Verić, O., Božić, Ž., Sušić, A., 2019. Fracture analysis of a total hip prosthesis based on reverse engineering. Engineering Fracture Mechanics 215, 261-271.

Babić, M., Verić, O., Božić, Ž., Sušić, A., 2020. Finite element modelling and fatigue life assessment of a cemented total hip prosthesis based on 3D scanning, Engineering Failure Analysis, 113, 104536.

Baragetti, S., 1997. Shot peening optimisation by means of 'DoE': Numerical simulation and choice of treatment parameters. International Journal of Materials and Product Technology 12, 83-109.

Baragetti, S., 2013. Corrosion fatigue behaviour of Ti-6Al-4V in methanol environment. Surface and Interface Analysis 45, 1654-1658.

Baragetti, S., Arcieri, E.V., 2019. Study on a new mobile anti-terror barrier. Procedia Structural Integrity 24, 91-100.

Baragetti, S., Arcieri, E.V., 2020. A new mobile anti-ramming system. ASME International Mechanical Engineering Congress and Exposition, Proceedings (IMECE) 14, 15960.

Baragetti, S., Arcieri, E.V., 2020. Study of impact phenomena for the design of a mobile anti-terror barrier: Experiments and finite element analyses. Engineering Failure Analysis 113, 104564.

Baragetti, S., Borzini, E., Arcieri, E.V., 2019. Quasi-static crack propagation in Ti-6Al-4V in inert and aggressive media. Corrosion Reviews 37, 533-538.

Baragetti, S., Borzini, E., Božić, Ž., Arcieri, E.V., 2019. Fracture surfaces of Ti-6Al-4V specimens under quasi-static loading in inert and aggressive environments. Engineering Failure Analysis 103, 132-143.

Baragetti, S., Borzini, E., Božić, Ž., Arcieri, E.V., 2019. On the fatigue strength of uncoated and DLC coated 7075-T6 aluminum alloy. Engineering Failure Analysis 102, 219-225.

Baragetti, S., Božić, Ž., Arcieri, E.V., 2020. Stress and fracture surface analysis of uncoated and coated 7075-T6 specimens under the rotating bending fatigue loading. Engineering Failure Analysis 112, 104512.

Baragetti, S., Gelfi, M., La Vecchia, G.M., Lecis, N., 2005. Fatigue resistance of CrN thin films deposited by arc evaporation process on H11 tool steel and 2205 duplex stainless steel. Fatigue & Fracture Engineering Materials & Structures 28, 615-621.

Baragetti, S., Terranova, A., 2000. Non-dimensional analysis of shot peening by means of DoE. International Journal of Materials and Product Technology 15, 131-141.

Božić, Ž., Schmauder, S., Mlikota, M., Hummel, M., 2014. Multiscale fatigue crack growth modelling for welded stiffened panels. Fatigue & Fracture Engineering Materials & Structures 37, 1043-1054.

Božić, Ž., Schmauder, S., Wolf, H., 2018. The effect of residual stresses on fatigue crack propagation in welded stiffened panels, Engineering Failure Analysis 84, 346-357.

Cazin, D., Braut, S., Božić Ž., Žigulić R., 2020. Low cycle fatigue life prediction of the demining tiller tool. Engineering Failure Analysis 111, 104457.

Condra, L.W., 1993. Reliability improvement with Design of Experiments. Marcel Dekker Inc., New York.

Mlikota M., Schmauder S., Božić Ž., Hummel M., 2017. Modelling of overload effects on fatigue crack initiation in case of carbon steel. Fatigue and Fracture of Engineering Materials and Structures 40(8), 1182–1190.

Mlikota, M., Schmauder, S., Božić, Ž., 2018. Calculation of the Wöhler (S-N) curve using a two-scale model. International Journal of Fatigue, 114, 289-297.

Nicholas, T., 2006. Foreign Object Damage in High Cycle Fatigue, Elsevier Science Ltd (Oxford).

Papadopoulou, S., Pressas, I., Vazdirvanidis, A., Pantazopoulos, G., 2019. Fatigue failure analysis of roll steel pins from a chain assembly: Fracture mechanism and numerical modeling. Engineering Failure Analysis 101, 320-328.

Pastorcic, D., Vukelic, G., Bozic, Z., 2019. Coil spring failure and fatigue analysis. Engineering Failure Analysis 99, 310-318.

Rølvåg, T., Haugen, B., Bella, M., Berto, F., 2020. Fatigue analysis of high performance race engines. Engineering Failure Analysis 112, 104514.

Solob, A., Grbović, A., Božić, Ž., Sedmak, S.A., 2020. XFEM based analysis of fatigue crack growth in damaged wing-fuselage attachment lug. Engineering Failure Analysis 112, 104516.

Voorwald, H.J.C., Bonora, R.G., Oliveira, V.M.C.A., Cioffi, M.O.H., 2019. Increasing fatigue resistance of AISI 4340 steel by nitrogen plasma ion-implantation. Engineering Failure Analysis 104, 490-499.